X-ray crystallographic and kinetic correlation of a clinically observed human fumarase mutation

MARCEL ESTÉVEZ,[1] JEREMY SKARDA,[2] JOSH SPENCER,[2] LEONARD BANASZAK,[3] AND TODD M. WEAVER[2]

[1]Johns Hopkins University, School of Medicine, Department of Neuroscience, Baltimore, Maryland 21205, USA
[2]University of Wisconsin–La Crosse, Department of Chemistry, La Crosse, Wisconsin 54601, USA
[3]University of Minnesota, Department of Biochemistry, Molecular Biology and Biophysics, Minneapolis, Minnesota 55455, USA

(RECEIVED January 9, 2002; FINAL REVISION March 15, 2002; ACCEPTED March 16, 2002)

Abstract

Fumarase catalyzes the reversible conversion of fumarate to *S*- malate during the operation of the ubiquitous Kreb's cycle. Previous studies have shown that the active site includes side chains from three of the four subunits within the tetrameric enzyme. We used a clinically observed human mutation to narrow our search for potential catalytic groups within the fumarase active site. Offspring homozygous for the missense mutation, a G-955–C transversion in the fumarase gene, results in the substitution of a glutamine at amino acid 319 for the normal glutamic acid. To more fully understand the implications of this mutation, a single-step site-directed mutagenesis method was used to generate the homologous substitution at position 315 within fumarase C from *Escherichia coli*. Subsequent kinetic and X-ray crystal structure analyses show changes in the turnover number and the cocrystal structure with bound citrate.

Keywords: Fumarase; active site; Kreb's cycle; homology; metabolic disease

Fumarases

Fumarase enzymes catalyze the reversible hydration/dehydration of fumarate to *S*-malate. Prokaroytes have three forms of fumarase, fumarase A, fumarase B, and fumarase C (FumC), and each has been classified as either class I or class II, depending on their relative subunit arrangement, metal requirement, and thermal stability. FumC belongs to the class II-type fumarases, which are iron-independent, thermal-stable, tetrameric enzymes of 200,000 D harboring three distinct segments of amino acids with significant homology. It is the focus of this study. Class I fumarases are heat-labile, superoxide anion radical (O_2^-)-sensitive, Fe^{2+}-dependent, dimeric proteins of 120 kD. Fumarase A and fumarase B from *Escherichia coli* (*E. coli*) are examples of class I fumarases.

There are two types of fumarase found within human tissues, cytosolic and mitochondrial, and both share sequence identity to FumC from *E. coli* (Woods et al. 1986). The mitochondrial form is responsible for the reversible conversion of fumarate to *S*-malate during operation of the Kreb's cycle, whereas the cytosolic form metabolizes fumarate, a by-product of the urea cycle.

Superfamily

Amino acid identity within the class II fumarase family is quite high, 59% between FumC from *E. coli* and human fumarase (Woods et al. 1986). In addition, this classification shows an elevated level of identity within three specific regions. Region 1 spans His 129 through Thr 146, region 2 Val 182 through Glu 200, and region 3 Gly 317 through Glu 331 (all amino-acid numbering is based on the FumC amino acid sequence unless otherwise noted).

FumC was the first class II fumarase enzyme structure to be solved, and its active site was shown to harbor many of the amino acids within the three highly conserved regions (Weaver et al. 1995). In particular, homology between Gly

Reprint requests to: Dr. Todd M. Weaver, University of Wisconsin–La Crosse, Department of Chemistry, La Crosse, WI 54601, USA; e-mail: weaver.todd@uwlax.edu; fax: (608) 785-8281.

Abbreviations: Ni^{2+}-NTA, nickel nitrotriloacetic acid; FumC, fumarase C.

Article and publication are at http://www.proteinscience.org/cgi/doi/10.1110/ps.0201502.

317 through Glu 331 within the third region has provided a signature sequence motif, which defines not only the class II fumarase family, but also a much broader superfamily of proteins. Although side chains from all three homologous regions are found in the active site, they are juxtaposed only in the tetramer.

The signature sequence (GSSxMPxKxNPxxxE) lying between Gly 317 and Glu 331 has provided a means to establish an evolutionary link between a broad superfamily of proteins, all but one of which are enzymes. Along with class II fumarases, members of the aspartase, arginosuccinate lyase, adenylosuccinate lyase, *cis*-muconate lactonizing enzyme, and δ-crystallin families also share significant amino acid homology in the signature sequence region. Figure 1 shows a sequence alignment of the 300s loop for various members of the fumarase superfamily.

This superfamily is characterized by a three-domained, dumbbell-shaped monomeric structure with a five-helix bundle at the core of the central second domain. Tetramer formation packs the five-helix bundle of the second domain from each monomer into a superhelical core. Whereas domain 2 forms the core of the tetramer, domains 1 and 3 extend off the top, bottom, and sides of the core unit.

Although the family members share high identity within the signature motif region, other segments are less well conserved. Just beyond the borders of the signature sequence, the identities tend to lessen across the superfamily, but stay relatively high within a single particular enzyme family. This is illustrated in Figure 1, where within a particular family, amino acid identities are maintained even beyond the signature sequence region. For example, Glu 315 is only conserved among the fumarase members, and in the other members of the superfamily, this position is occupied by Gln (aspartase and adenylosuccinate members) and Ser or Cys (argininosuccinate lyase). The divergence at this position within the superfamily may indicate a selective role for Glu 315 during the fumarase catalytic reaction.

Inborn error

In humans, two sisters' progressive psychomotor retardation, failure to thrive, microcephaly, and abnormal posture with hypotonia contrasting with hypertonia of limbs, all indicative of a progressive metabolic encephalopathy, have been attributed to an inborn error of fumarase. On further examination, these siblings were found to have elevated levels of lactate in their cerebrospinal fluid and high fumarate excretion in their urine. This led the investigators to focus on activities involved in the respiratory chain of the Kreb's cycle. The deficiency within these two siblings, born to first cousins, was finally attributed to the inactivity of both cytosolic and mitochondrial forms of fumarase.

	312			315																331
Fumarase				↓		*	*	*		*	*		*		*	*				*
E.coli	P	E	N	**E**	P	*G*	*S*	*S*	*I*	*M*	*P*	*G*	*K*	*V*	*N*	*P*	*T*	*Q*	*C*	*E*
Rat	P	E	N	**E**	P	*G*	*S*	*S*	*I*	*M*	*P*	*G*	*K*	*V*	*N*	*P*	*T*	*Q*	*C*	*E*
Human	P	E	N	**E**	P	*G*	*S*	*S*	*I*	*M*	*P*	*G*	*K*	*V*	*N*	*P*	*T*	*Q*	*C*	*E*
Yeast	P	E	N	**E**	P	*G*	*S*	*S*	*I*	*M*	*P*	*G*	*K*	*V*	*N*	*P*	*T*	*Q*	*N*	*E*
Aspartase																				
E.coli	P	E	L	Q	A	*G*	*S*	*S*	*I*	*M*	*P*	*A*	*K*	*V*	*N*	*P*	*V*	*V*	*P*	*E*
S.marcescens	P	E	L	Q	A	*G*	*S*	*S*	*I*	*M*	*P*	*A*	*K*	*V*	*N*	*P*	*V*	*V*	*P*	*E*
P.fluorescens	P	A	R	Q	P	*G*	*S*	*S*	*I*	*M*	*P*	*G*	*K*	*V*	*N*	*P*	*V*	*I*	*P*	*E*
B.subtilis	P	A	R	Q	P	*G*	*S*	*S*	*I*	*M*	*P*	*G*	*K*	*V*	*N*	*P*	*V*	*M*	*A*	*E*
Arginosuccinate lyase																				
Human	D	A	Y	S	T	*G*	*S*	*S*	*L*	*M*	*P*	*Q*	*K*	*K*	*N*	*P*	*D*	*S*	*L*	*E*
Rat	D	A	Y	S	T	*G*	*S*	*S*	*L*	*M*	*P*	*Q*	*K*	*K*	*N*	*P*	*D*	*S*	*L*	*E*
Goose	D	A	F	S	T	*G*	*S*	*S*	*L*	*M*	*P*	*Q*	*K*	*K*	*N*	*P*	*D*	*S*	*L*	*E*
Pigeon	D	T	Y	C	T	*G*	*S*	*S*	*V*	*M*	*P*	*Q*	*K*	*K*	*N*	*P*	*D*	*S*	*L*	*E*
Yeast	D	A	Y	S	T	*G*	*S*	*S*	*L*	*M*	*P*	*Q*	*K*	*K*	*N*	*A*	*D*	*S*	*L*	*E*
Adenylosuccinate Lyase																				
Chicken	E	K	D	Q	I	*G*	*S*	*S*	*A*	*M*	*P*	*Y*	*K*	*R*	*N*	*P*	*M*	*R*	*S*	*E*
E.coli	I	A	G	E	I	*G*	*S*	*S*	*T*	*M*	*P*	*H*	*K*	*V*	*N*	*P*	*I*	*D*	*F*	*E*
B.subtilis	A	K	G	Q	K	*G*	*S*	*S*	*A*	*M*	*P*	*H*	*K*	*R*	*N*	*P*	*I*	*G*	*S*	*E*
δ-crystallin II																				
Chicken	D	A	Y	S	T	*G*	*S*	*S*	*L*	*L*	*P*	*Q*	*K*	*K*	*N*	*P*	*D*	*S*	*L*	*E*

Fig. 1. Superfamily 300s loop sequence alignment. The sequence alignment shows identity within the 300s loop region of the superfamily members, fumarase, aspartase, adenylosuccinate lyase, arginosuccinate lyase, and δ-crystallin. Each distinct family of sequences has been grouped and identified within the alignment. The alignment is numbered based on *E. coli* fumarase C, where the italicized region identifies the signature sequence spanning Gly 317 through Glu 331. (↓) Glu 315; (*) identical amino acids within the superfamily signature sequence; (Yeast) *Saccharomyces cerevisiae*; (*E. coli*) *Escherichia coli*; (*S. marcescens*) *Serratia marcescens*; (*P. fluorescens*) *Pseudomonas fluorescens*; (*B. subtilis*) *Bacillus subtilis*.

This deficiency extended to all tissues tested for fumarase activity. The sisters were found to be homozygous for a missense mutation at position 955. The G to C transversion at position 955 equates to the substitution of a glutamine at amino acid position 319 (numbering based upon human fumarase) for the normal glutamic acid (Bourgeron et al. 1994). The first-cousin parents showed half the expected fumarase activity when their tissue extracts were analyzed, and they were found to be identically heterozygous for a substitution at position 955. Glu 319, in the human fumarase amino acid sequence, is homologous to Glu 315 in *E. coli* FumC, and is located near the highly conserved signature sequence region of amino acids residing within the active site.

To understand the consequences attributed to the glutamic acid to glutamine mutation at position 319 in human fumarase, we engineered a homologous substitution in *E. coli* FumC. The result of replacing Glu 315 with a glutamine within FumC has been characterized kinetically and crystallographically. The kinetic data indicate an ~10-fold reduction in catalytic efficiency during the reversible reaction, whereas the X-ray crystallographic data implicate the loss of an active-site water molecule as the potential reason for the decrease in efficiency.

Results and Discussion

Screening for E315Q

Six colonies subjected to *Bam*HI restriction digestion confirmed the incorporation of the additional restriction site as designed within the oligonucleotide primers. Subsequent DNA sequencing results established that the only point of alteration within the *fumc* gene sequence was the engineered position at base 945. Overall 1 g of purified E315Q was obtained from 60 g of *E. coli* cell paste using the Ni^{2+}-NTA metal-chelate chromatography as supplied by QIAGEN.

Kinetic characterization of E315Q

FumC, like other members of the fumarase family, catalyze the reversible dehydration/hydration of *S*-malate to fumarate. The steady-state kinetic investigations have analyzed the mutant and native forms of fumarase during both the dehydration and hydration events. Table 1 contains a summary of the kinetic constants for both native and E315Q forms of FumC. As is indicated in Table 1, there is essentially no effect of the glutamine for glutamic acid substitution at position 315 on the K_m values for both *S*-malate and fumarate. In contrast, the k_{cat} values for E315Q have been lowered by ~10-fold in both directions. Overall, the catalytic efficiency has been lowered 11-fold in the *S*-malate to fumarate direction and 13-fold in the fumarate to *S*-malate direction.

Table 1. *Kinetic summary for native FumC and E315Q*

Enzyme	Native	E315Q
S-malate → fumarate		
V_{max} (μmol substrate/min/mg enzyme)	178.6	16.11
K_m (mM)	0.857	0.885
k_{cat} (s^{-1})	595.2	55.32
k_{cat}/K_m (M^{-1} s^{-1})	6.95E5	6.25E4
Fumarate → *S*-malate		
V_{max} (μmol substrate/min/mg enzyme)	344.8	32.2
K_m (mM)	0.207	0.248
k_{cat} (s^{-1})	1149	107.1
k_{cat}/K_m (M^{-1} s^{-1})	5.56E6	4.32E5

X-ray crystallographic characterization of E315Q

The coordinates for native FumC (1FUO) were used as a starting model for the refinement scheme, wherein Glu 315 was replaced with an alanine side chain, and all ligand and solvent molecules were excluded. There were two major perturbations within the mutant active site. The first obvious alteration is localized within the substituted glutamine side chain. Gln 315 adopts a conformation whereby the hydrogen bond once shared between glutamic acid 315 and Thr 328 appears absent.

The second and more indirect effect of the substitution at position 315 is the absence of electron density for a conserved and highly coordinated active-site water molecule (Weaver et al. 1997). Figure 2, A and B, provides ball-and-stick models for both E315Q and native FumC, which emphasize the position of Gln 315 and Glu 315, respectively. In addition, the relative position of the active-site water (W54) within the native FumC active site is illustrated in Fig. 2A. From the crystallographic model and electron density map it is not exactly clear why the highly coordinated active site water is no longer bound, but $2|F_o| - |F_c|$ and $|F_o| - |F_c|$ maps contoured at 1.0 σ and 3.0 σ, respectively, are not indicative of misplaced side chains or solvent electron density within this region of the active site. Typically, the active-site water is one of the top peaks during solvent placement and is clearly absent from the resulting E315Q electron density maps.

To date there are two distinct native crystal structures of FumC with the reported active-site water. The first, a C-centered orthorhombic habit was crystallized at low pH in the presence of 150 mM citrate (a competitive inhibitor of FumC), whereas the second form, an I-centered orthorhombic habit, was crystallized at neutral pH devoid of inhibitors (Weaver et al. 1993). In both refined crystal structures, the active-site water was observed to form a network of hydrogen bonds to His 188, Asn 141, Ser 98, and Thr 100 deep within the active site. In the case of the C-centered orthorhombic habit, the water is positioned in close proximity to the bound competitive inhibitor citrate.

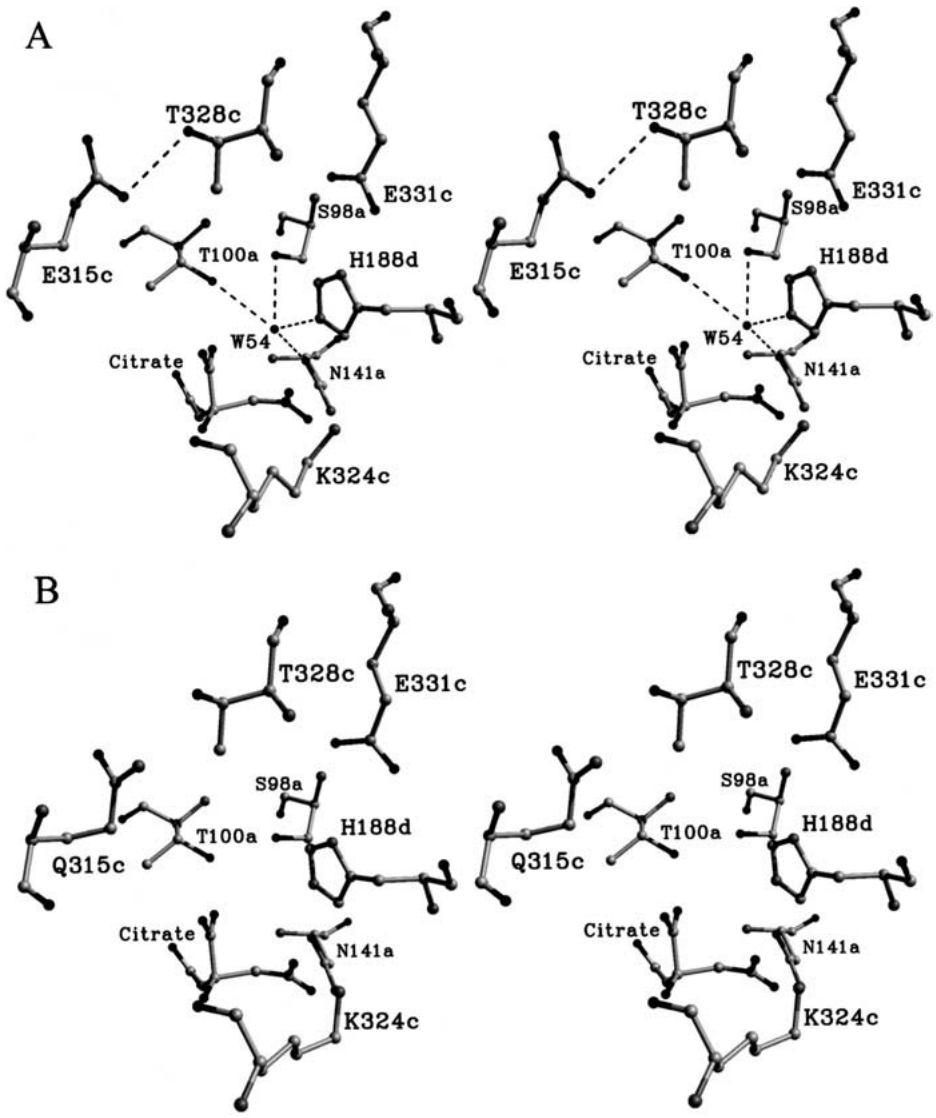

Fig. 2. Structural comparisons between native and E315Q fumarase active sites. (*A*) The native FumC active site illustrating the positions of Glu 315, citrate, and the highly coordinated active-site water (W54). (*B*) The E315Q active site with the positions of Gln 315 and citrate and the absence of W54. Dashed lines are hydrogen bonds. Atoms are shaded as follows: carbon, light gray; oxygen, black; and nitrogen, dark gray. Amino acids are labeled using the one-letter code with E, glutamic acid; K, lysine; N, asparagines; Q, glutamine; S, serine; T, threonine; and H, histidine. Subunit designation is provided by the lowercase letter following the amino acid number.

In the I-centered habit, the water molecule still is found in approximately the same position even though the active site is devoid of bound citrate. Therefore, the binding of the active-site water does not seem to be a result of crystallization conditions. In fact, W54 has been observed in all of the previously reported FumC crystals structure (1FUP; 1FUQ; 1FUR; 2FUS).

Replacement of a carboxylate at position 315 for a carboxyamide in this study has effectively displaced a highly coordinated water molecule within the active site, and this effect is reflected in the ~10-fold reduction in k_{cat} in both the hydration and dehydration events.

The combination of the past crystallographic data on FumC with the more recent analysis of E315Q seems to indicate that the previously reported crystal structures of FumC describe the fumarate specific conformer. In this form, W54 is the active-site water used to hydrate the olefinic bond of fumarate.

Previous investigations have also indicated different conformers for fumarase (Rose 1998; Rebholz and Northrup 1994). Although Glu 315 does share identity among the superfamily members, it does harbor absolute identity with the fumarase members, as illustrated in Figure 1. Based on this and past X-ray investigations, Glu 315 does position

itself within the fumarase C active site near a previously observed active-site water molecule. The kinetic data provide evidence that the glutamine replacement at position 315 has little effect on substrate binding. Rather, the mutation directly decreases the efficiency of the catalytic reaction. The 10-fold reduction in k_{cat} probably does not support Glu 315 as the as-yet-elusive catalytic acid, but the resulting X-ray structure does implicate the importance of this side chain in maintaining the proper architecture within the fumarate selective conformer active site. Collectively, the kinetic and crystallographic data for E315Q indicate that the carboxyamide replacement at position 315 inactivates FumC by perturbing the active site, thereby elevating the subsequent K_m for the bound water.

Materials and methods

Mutagenesis

A set of oligonucleotide primers was designed to incorporate the G-945–C transversion, along with an additional *Bam*HI restriction site. The upper primer sequence is CCGGAAAATCAGCCG*G GATCC*TCAATCATGCC; the lower primer sequence is GGCAT GATTGAGGATCCCGGCTGATTTTCCGG. The underlined bases indicate the glutamine side-chain replacement at position 315, and the italicized region describes the newly engineered *Bam*HI restriction endonuclease site. The *Bam*HI site allowed for rapid identification of the mutant clones. Site-directed mutagenesis experiments were carried out according to the QuikChange Kit as designed by Stratagene. The mutant *fumC* gene was subjected to automated DNA sequencing, and the only position of alteration was that at position 945.

Protein preparation and crystallization

E315Q FumC was purified via metal-chelate chromatography as previously described (Weaver et al. 1997). E315Q was pooled and concentrated to 57.5 μM using an Amicon stir cell fitted with a YM-30 membrane. Following concentration, E315Q was dialyzed against two successive 4-L volumes of 20 mM Tris-HCl (pH 7.5), 5 mM DTT, and 5 mM EDTA. E315Q crystals were grown out of a solution containing 150 mM sodium citrate (pH 5.6) and 14% PEG 3350.

Kinetic analysis

Enzyme activity was measured by monitoring the conversion of either *S*-malate to fumarate or fumarate to *S*-malate at 250 nm. The conversion of *S*-malate to fumarate was monitored at 250 nm by an increase in absorbance, whereas the conversion of fumarate to *S*-malate was monitored by a decrease in absorbance at 250 nm. For standard enzyme activity measurements during purification, the assays were performed using 20 mM Tris-HCl (pH 7.9) and 50 mM *S*-malate. To ascertain the apparent kinetic constants of the enzymatic conversions, including K_m, V_{max}, and k_{cat} values, native FumC and E315Q activity was measured at varying *S*-malate and fumarate concentrations. Table 1 summarizes the kinetic data for native FumC and E315Q.

Table 2. *Refinement statistics for E315Q FumC*

Dataset	E315Q
Resolution - Å	8.0–2.6
R_{free}	25.1
R_{factor}	17.9
No. Reflections I/σ(I)	21262
Protein Atoms	6914
Water Molecules	18
Ligand Atoms	42
R.m.s.d. lengths-Å	0.007
R.m.s.d. angles°	1.261
R.m.s.d. dihedrals°	21.057
R.m.s.d. impropers°	1.269

X-ray data collection and refinement

The X-ray dataset was collected at room temperature using a Siemens-Nicollet area detector and a monochromatic source from a graphite crystal-CuK_α (λ = 1.542 Å). X-rays were generated using a rotating anode operating at 45 kV and 200 mA. Two crystals were used for the complete dataset collected to 2.6-Å resolution. The X-ray data were merged and scaled with the XENGEN suite of programs (Howard et al. 1987). The final E315Q dataset was 93.5% complete to 2.5 Å and had an $I/\sigma(I)$ of 10.28 for data between 13- and 2.5-Å resolution with an R_{merge} of 11.2.

To start the refinement scheme using the 1FUO coordinates, 100 cycles of Powell minimization were used, where Glu 315 was initially replaced with an alanine side chain. After the initial Powell minimization, a round of simulated annealing including the bulk solvent correction was performed within XPLOR version 3.8 (Brünger et al. 1987). A grouped B-factor refinement procedure was performed following the simulated annealing run. Mut_Rep and Tor_Res were used within the program O to position Gln 315 in the final electron density map (Jones et al. 1991). Water molecules obeying proper hydrogen-bonding constraints with electron densities >1 σ on a $2|F_o| - |F_c|$ map and 4 σ on an $|F_o| - |F_c|$ map were also included as the model neared completion. Table 2 lists the final refinement statistics for the E315Q crystal structure. The representative coordinate file has been deposited at the Protein Data Bank with the identification code 1KQ7.

Acknowledgments

The authors are grateful to Ed Hoeffner for his contributions to this study through the maintenance of the X-ray facilities at the University of Minnesota. In addition, the authors acknowledge the indirect help of Bob Milius for the software maintenance of the Biomedical Science Computer Laboratory at the University of Minnesota, an outstation of the Minnesota Supercomputer Institute. M.E. acknowledges support from the University of Minnesota through its *Life Sciences Summer Undergraduate Research Programs*. The project was supported in part by a grant from the National Science Foundation (MCB 9603656) to L.B. and a grant from the University of Wisconsin–La Crosse Faculty Research Program to T.W.

The publication costs of this article were defrayed in part by payment of page charges. This article must therefore be hereby marked "advertisement" in accordance with 18 USC section 1734 solely to indicate this fact.

References

Bourgeron, T., Chretien, D., Poggi-Bach, J., Doonan, S., Rabier, S., Letouzé, P., Munnich, A., Rötig, A., Landrieu, P., and Rustin, P. 1994. Mutation of the fumarase gene in two siblings with progressive encephalopathy and fumarase deficiency. *J. Clin. Invest.* **93:** 2514–2518.

Brünger, A.T., Kuriyan, J., and Karplus, M. 1987. Crystallographic R-factor refinement by molecular dynamics. *Science* **235:** 485–460.

Howard, A.J., Gilliland, G.L., Finzel, B.C., Poulos, T.L., Ohlendorf, D.H., and Salemme, F.R. 1987. The use of imaging proportional counter in macromolecular crystallography. *J. Appl. Cryst.* **20:** 383–387.

Jones, T.A., Zou, J.Y., Cowan, S.W., and Kjieldgaard, M. 1991. Improved methods for building protein models in electron density maps and the location of errors in these models. *Acta Crystallogr.* **A47:** 110–119.

Rebholz, K.L. and Northrup, D.B. 1994. Kinetics of enzymes with iso-mechanisms: Dead-end inhibition of fumarase and carbonic anhydrase II. *Arch. Biochem. Biophys.* **12:** 227–233.

Rose, I.A. 1998. How fumarase recycles after the malate → fumarate reaction. Insights into the reaction mechanism. *Biochemistry* **37:** 17651–17658.

Weaver, T.M., Levitt, D.G., and Banaszak, L.J. 1993. Purification and crystallization of fumarase C from *Escherichia coli*. *J. Mol. Biol.* **231:** 141–144.

Weaver, T.M., Levitt, D.G., Donnelly, M.I., Wilkens-Stevens, P.P., and Banaszak, L.J. 1995. The multisubunit active site of fumarase C from *Escherichia coli*. *Nat. Struct. Biol.* **2:** 654–662.

Weaver, T.M., Lees, M., and Banaszak, L.J. 1997. Mutations of fumarase that distinguish between the active site and a nearby dicarboxylic acid binding site. *Protein Sci.* **6:** 834–842.

Woods, S.A., Miles, J.S., Roberts, R.E., and Guest, J.R. 1986. Structural and functional relationships between fumarase and aspartase. *Biochem. J.* **237:** 547–557.